Electrochemical Monitoring of TiO$_2$ Atomic Layer Deposition by Chronoamperometry and Scanning Electrochemical Microscopy

Ashis K. Satpati,[§,†,‡] Netzahualcóyotl Arroyo-Currás,[§,‡] Li Ji,[§,∥,⊥] Edward T. Yu,[∥,⊥] and Allen J. Bard*,[§]

[§]Center for Electrochemistry, Department of Chemistry and Biochemistry, [∥]Texas Materials Institute and the Materials Science and Engineering Program, The University of Texas at Austin, Austin, Texas 78712, and [⊥]Microelectronics Research Center, The University of Texas at Austin, Austin TX 78758, United States

S *Supporting Information*

ABSTRACT: The scanning electrochemical microscope (SECM) was used to characterize the atomic layer deposition (ALD) of TiO$_2$ on indium-doped tin oxide (ITO) substrates by studying electron transfer through pores in the thin films (1−5 nm thickness). The extent of electron transfer, and thus the porosity of the films, was evaluated by transient electrochemistry. These studies show that ALD deposition of TiO$_2$ on ITO does not produce pinhole-free films but rather porous deposits with electrochemical behavior similar to that of microelectrode arrays up to about 30 ALD cycles. All the experimental results are explained in the context of a numerical model developed by finite element analysis and corroborated by complementary conductive atomic force microscopy (cAFM) results that directly reveal localized, nanoscale current conduction paths in thinner TiO$_2$ layers with a transition to more spatially uniform conduction in the thickest layers. SECM images demonstrate the existence of pinholes even on films that have been subjected to more than 100 ALD cycles (thicknesses larger than 4 nm).

KEYWORDS: *atomic layer deposition (ALD), scanning electrochemical microscopy (SECM), nanoporous films, finite element modeling*
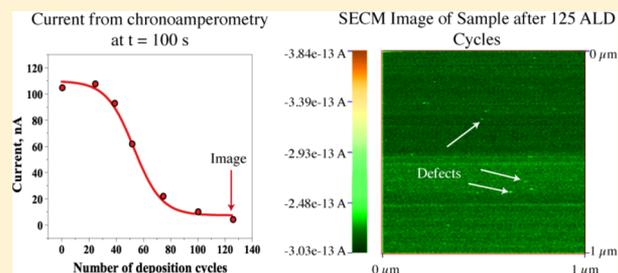
■ INTRODUCTION

We carried out experiments with the scanning electrochemical microscope (SECM)[1] to characterize TiO$_2$ films created by atomic layer deposition (ALD)[2] on indium-doped tin oxide (ITO) substrates. In particular, we evaluated electron transfer at TiO$_2$-coated ITO at different stages of surface coverage and in films of different thicknesses (δ = 1−5 nm). SECM is a useful technique for the localized evaluation of charge transfer across thin films because it allows discrimination between currents tunneling through a film and those associated with pinholes.[3]

ALD, or atomic layer epitaxy (ALE), was developed in the 1970s.[4] This technique is believed to form pinhole-free, atomically smooth conformal deposits on even and uneven substrates, thanks to its sequential and self-limiting type of reaction mechanism.[5] In the semiconductor industry, ALD has been used as a standard method to deposit the diffusion barrier in metal−oxide−semiconductor field-effect transistor (MOS-FET) structures.[6] Since the semiconductor industry has undergone miniaturization in many specific applications, the requirement of producing conformal coatings with a high aspect ratio has become critically important.[7] ALD is the preferred choice over other deposition techniques for conformal coating on miniaturized devices. Furthermore, ALD plays an important role in the deposition of thin oxide films with high dielectric constants like HfO$_2$ and SrTiO$_3$ for electronic applications,[8] as well as ZnO, TiO$_2$, and Al$_2$O$_3$ for electrical, mechanical, electrochemical, and optical applications.[9−18] In the context of

photoelectrocatalysis, a recent publication has employed ALD deposition of TiO$_2$ on Si wafers to produce a robust photoanode for photoelectrochemical water oxidation.[16] The transparent oxide coatings deposited by ALD on various semiconductor materials may play an important role in reducing photocorrosion and electrochemical decomposition of the photocatalyst, e.g., in water splitting experiments. Some important reviews on the mechanism of ALD deposition and its use in different fields are available.[19−26]

We were interested in studying the extent of electron transfer through oxide films deposited by ALD as a function of the number of applied cycles. ALD is known to be a slow process, with deposition rates of 100−300 nm h^{-1} (only a fraction of a monolayer per pulse).[27] Even though characterization of ALD deposits has traditionally been performed by spectroscopic methods, electrochemistry is a more suitable tool for the monitoring of charge transfer at such deposits. To the best of our knowledge, such electrochemical studies of electron transfer through ALD thin films have not been reported. Here, we discuss the ALD deposition of TiO$_2$ on ITO substrates by multiple deposition cycles to produce different thicknesses and surface coverage. Electron transfer with the TiO$_2$ films was investigated by chronoamperometry and voltammetry, and the

results treated by a model developed by finite element analysis. SECM experiments were also carried out to study charge transport at localized surface regions, and to detect the presence of pinholes in the films. These results were corroborated by

conductive atomic force microscopy (cAFM) imaging and spectroscopy that provide direct evidence of localized variations in conduction at submicrometer length scales and a transition from highly localized to more spatially uniform conduction with increasing TiO_2 layer thickness.

Table 1. Conversions between Film Thickness (δ) and Number of ALD Pulses Applied[a]

δ (nm)	no. of pulses
1.00	25
1.52	38
2.00	50
3.00	75
4.00	100
5.00	125

[a]Conversion factor = 0.04 nm/pulse.
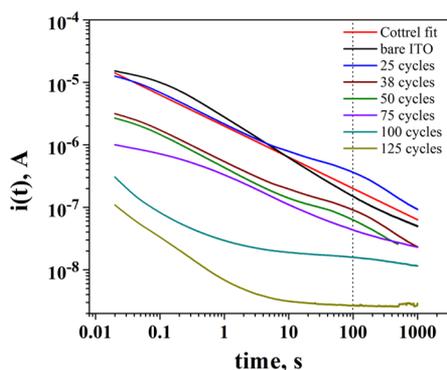
Figure 1. Chronoamperograms of 1 mM FcMeOH in 0.1 M KNO_3 solution at TiO_2-covered ITO, logarithmic scale. E_{app} = 0.5 V ($E^{0'}$ = 0.24 V vs Ag/AgCl). The vertical dashed line represents the time, t = 100 s, at which current was sampled to make Figure 4.

■ EXPERIMENTAL SECTION

Instrumentation. A Savannah ALD system from Cambridge Nanotech (Cambridge, MA) was used for the deposition of TiO_2 films. The instrument was calibrated to deposit 0.04 nm thick TiO_2 films per cycle. ITO plates were obtained from Delta Technologies Ltd. (Loveland, CO). Scanning electron microscopy (SEM) measurements were carried out with a Hitachi S-5500 (Dallas, TX) to qualitatively characterize the deposits. All electrochemical measurements were carried out with a CHI920C SECM workstation from CH Instruments (Austin, TX). A three-electrode cell configuration was used during all electrochemical measurements. In chronoamperometric measurements the working electrode (ALD sample or array sample) was clamped over a hole in the bottom of the Teflon sample cell with the exposed radius defined by the rubber O-ring (r = 0.35 cm). The counter electrode was a platinum wire. Potentials in this work are reported vs Ag/AgCl reference electrode.

SECM measurements were carried out in the same cell. The 10 μm diameter platinum wire was purchased from Alfa Aesar (Wardhill, MA) to fabricate SECM tips by the methods described elsewhere.[1] All SECM tips had RG = 2.0 ± 0.1. Dr. Sun Peng from East Tennessee State University kindly donated the nanoelectrode used for the detection of pinholes in this work (Pt, 86 nm diameter, RG = 1.1 ± 0.1). Ferrocenemethanol (FcMeOH) and potassium nitrate (KNO_3) were purchased from Thermo Fischer Scientific (New Jersey) and used as received. Solutions were prepared using a Milli-Q water system (18 MΩ). cAFM measurements were performed using a Bruker Dimension Icon AFM system (Bruker Co., Germany) with diamond coated, antimony doped silicon probe tips (DDESP-FM-10, Bruker Co., Germany) in the contact mode.
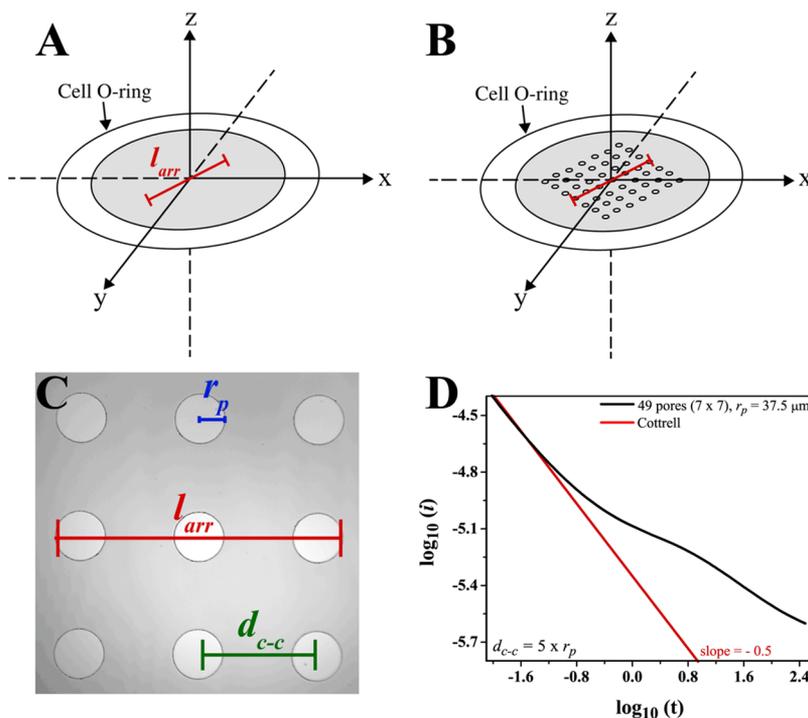
Figure 2. (A) Simplified geometry of an inlaid disk electrode with r_{arr} = 600 μm. (B) Same geometry as in A but with an ideal microarray of electrodes generated after 25 ALD pulses. (C) Optical image of a geometry-controlled substrate fabricated and used to validate the numerical model. (D) Numerical simulation of chronoamperograms of 1 mM FcMeOH for the geometry shown in A (red line) and for that shown in B (black line). An array of 49 microelectrodes behaves similarly to an experimental substrate after 25 ALD cycles of TiO_2 on ITO.
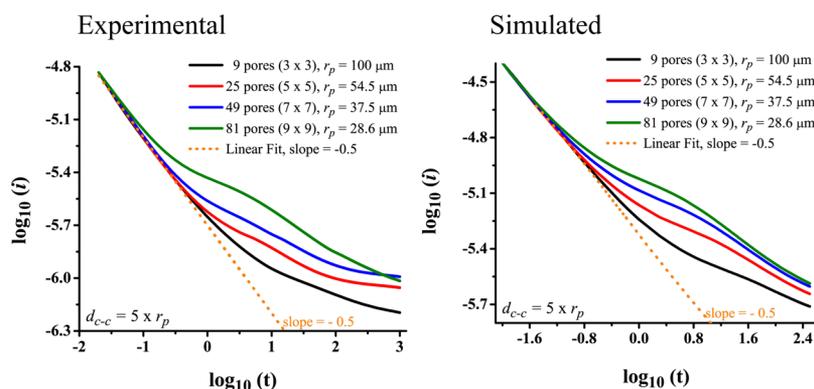
Figure 3. Experimental and simulated chronoamperograms for 1 mM FcMeOH oxidation in 0.1 M KNO₃ solution at geometry-controlled substrates.

Preparation of Substrates for ALD. As received ITO plates were first sonicated in water (10 min) and then in ethanol (30 min) and finally dried in an oven at 120 °C for 10 min. The cleaned ITO plates were placed inside the ALD chamber. Tetrakis(dimethylamido) titanium (TDMAT) was used as the precursor. The precursor cylinder was kept at 75 °C for evaporation, and the deposition chamber was maintained at 150 °C. Detailed deposition parameters are tabulated in Scheme S1 of the Supporting Information. An ALD deposition scheme for a similar system was previously reported.[28] On precursor pulsing, TDMAT molecules were adsorbed over the ITO substrate by releasing two molecules of dimethylaniline. On water pulsing, the two remaining dimethylamido groups were released leaving two unbound OH groups in the Ti center, which were available for the adsorption of TDMAT molecules arriving on repetitive precursor pulsing. The net chemical reaction scheme that produced the TiO₂ deposition was

$$[(CH_3)_2N]_4Ti + 2H_2O \rightleftharpoons TiO_2 + 4(CH_3)_2NH$$

Desorbed TDMAT molecules decompose through various reactions described previously; these reaction products are nonabsorbable and flowed out of the reaction chamber by the carrier gas.[29,30] The number of deposition cycles, or pulses, was carefully controlled to produce films with different thicknesses and surface coverage (step 14 in Supporting Information Scheme S1). The produced deposits were qualitatively examined by SEM and X-ray photoelectron spectroscopy (XPS). In selecting a substrate, we initially evaluated the quality of TiO₂ films deposited by ALD on four different substrates: Ag, Pt, fluorine-doped tin oxide coated glass (FTO), and ITO coated glass. Pt (30 nm thickness) and Ag (65 nm thickness) smooth surfaces were prepared prior to ALD treatment by sputtering and chemical vapor deposition on Si substrates, respectively. Preliminary XPS/SEM results showed that the best films were produced on ITO substrates (see Figures S1−S7 in the Supporting Information); hence, we limited the studies here to only TiO₂ on ITO.

Preparation of Samples for Testing the Theoretical Model. The results from chronoamperometry presented in this work are explained within the context of a model created by both theoretical and experimental analysis. The theoretical model was developed using commercial software (COMSOL Multiphysics version 4.2) based on finite element methods (FEM). The experiments were carried out on geometry-controlled samples that mimicked the geometry employed in the simulations. Such samples were produced by soft lithography[31] with methods explained elsewhere.[32] Briefly, a layer of positive photoresist (1 mL, ∼10 µm thick, AZ P4620, AZ Electronic Materials, Somerville, NJ) was spin-coated onto a Au coated glass slide (EMF Corp., Ithaca, NY) and then exposed to UV light through positive photomasks containing the electrode microarray designs. The photomasks were created with Corel Draw Graphics Suit 12 and printed at CAD/Art Services, Inc. (Bandon, OR). The electrode microstructures were transferred to the Au slides by developing the photoresist in AZ 421 K solution (AZ Electronic Materials, Somerville, NJ) for 2 min.

Table 2. Conversions between Film Thickness (δ) and Number of ALD Pulses Applied[a]

no. of ALD cycles	type of diffusion during time transient			parameters
	0.01 s ≤ t ≤ 1 sl	1 s ≤ t ≤ 100 s	t ≥ 100 s	
25	linear	linear to steady-state	linear	$d_{c-c} \leq 15r_p$, $r_p = \mu m$
38	linear	linear to steady-state	linear	$d_{c-c} \leq 15r_p$, $r_p = \mu m$
50	linear	linear to steady-state	linear	$d_{c-c} \leq 15r_p$, $r_p = \mu m$
75	steady-state to linear	linear to steady-state	steady-state	$d_{c-c} \leq 5r_p$, $r_p < \mu m$
100	steady-state	steady-state	steady-state	$d_{c-c} \leq 30r_p$, $r_p < nm$
125	steady-state	steady-state	steady-state	$d_{c-c} \geq 30r_p$, $r_p < nm$

[a]Conversion factor = 0.04 nm/pulse.

Optical images of these samples are provided in Supporting Information Figure S8. The substrates had an overall radius defined by the O-ring at the cell bottom that defined the area; the arrays with 9, 25, 49, and 81 pores were always centered. Each individual pore within an array was a recessed gold microelectrode surrounded by 10 µm thick insulating photoresist.

■ RESULTS AND DISCUSSION

The problem of electron transfer through thin films at the solid−electrolyte interface has been studied extensively for the case of self-assembled monolayers (SAM) of alkane thiols and oxide films.[33] When no pinholes or defects are present (an ideal situation), electrons can tunnel through a film at a rate that decays exponentially with distance:[33,34]

$$k^0(x) = k^0(x = 0)e^{-\beta x}$$

where x is the distance over which tunneling occurs and β is a kinetic factor that depends weakly on potential. However, if pinholes or imperfections are present in the film, the extent of electron transfer also becomes a function of the size and distribution of pores after the assembly/deposition process. This is precisely the case observed for TiO₂ films generated by ALD on ITO at coverages below 100 deposition cycles ($\delta \leq 4$ nm, see Table 1). Within that thickness range, electrochemical measurements carried out on TiO₂-covered substrates showed no tunneling behavior but rather an electrochemical response that could easily be correlated to the architecture of a film that is porous in nature.

Chronoamperometric Analysis. Potentiostatic measurements were carried out with the oxidation of 1 mM FcMeOH in 0.1 M KNO_3 solution at an applied potential, E_{app} = 0.5 V ($E^{0'}$ = 0.24 V vs Ag/AgCl), for 1000 s. The chronoamperograms obtained are shown in Figure 1. In the figure, the $\log_{10} i(t)$ recorded at a bare ITO electrode of area = 0.38 cm^2 (TiO_2-free surface, black line) showed Cottrell behavior (eq 1) with a slope $m = -0.59 \pm 0.05$ (compared to theoretical $m_{Cottrell}$ = −0.5, red line).

$$\log_{10} i(t) = \log_{10} \frac{nFAD^{1/2}C}{\pi^{1/2}} - \frac{1}{2}\log_{10} t \tag{1}$$

As the deposition of TiO_2 increased with the number of ALD cycles applied, the initial magnitude of $\log_{10} i(t)$ decreased proportionally to the extent of surface coverage. Also, different transitions in current behavior were observed in each of the substrates produced. For example, the chronoamperogram corresponding to 25 ALD cycles (blue line) presented a $\log_{10} i(t)$ that first followed Cottrell behavior, then transitioned into a region of smaller slope (a *quasi* steady-state region), and then transitioned back into a second Cottrell decay region. Similar transitions were recorded at substrates produced after 38 and 50 ALD cycles. For deposits obtained after 75 ALD cycles or more, steady-state behavior was observed at $t \geq 100$ s. This electrochemical behavior is typically observed in microelectrode arrays, where mass transfer of electroactive species at one ultramicroelectrode region is time-dependent and affected by the presence of other neighboring ultramicroelectrodes.[35−41]

The problem of ALD fractional coverage can be treated by FEM in a simplified geometry like the one shown in Figure 2. The reaction considered in this work is:

Figure 4. Plot of $i(t = 100$ s) vs number of ALD deposition cycles for TiO_2 on ITO.
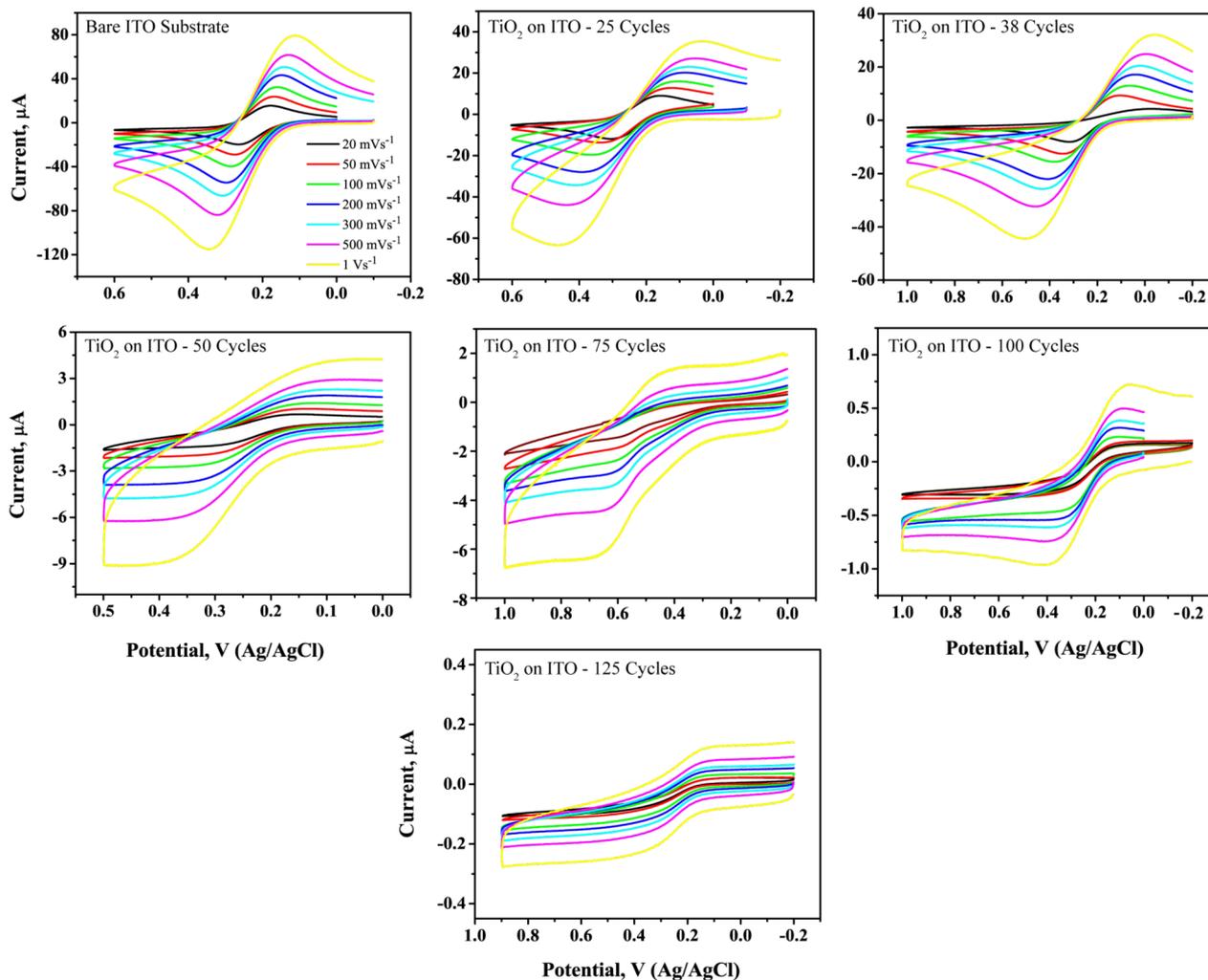
Figure 5. Cyclic voltammograms of 1 mM FcMeOH in 0.1 M KNO_3 solution at each of the substrates prepared. The colors correspond to scan rates of 20, 50, 100, 200, 300, 500, and 1000 mV s^{-1}. The color code is the same for all panels.

$$FcMeOH^+ + e^- \underset{k_b}{\overset{k_f}{\rightleftharpoons}} FcMeOH$$
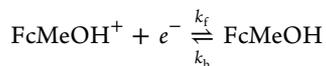
where k_f and k_b are rate constants defined according to the Buttler−Volmer formalism as

$$k_f = k^0 \exp^{[-\alpha f(E-E^0)]}$$

$$k_b = k^0 \exp^{[(1-\alpha)f(E-E^0)]}$$

The heterogeneous rate constant is $k^0 = 2$ cm s^{-1},[42] α is the transfer coefficient ($\alpha = 0.5$ in this work), and $f = F/RT$, where F is Faraday's constant, R the gas constant, and T the experimental temperature. The diffusion profile of electroactive species is calculated by solving Fick's second law in Cartesian coordinates for a three-dimensional geometry:

$$\frac{\partial C}{\partial t} = D\left(\frac{\partial^2 C}{\partial x^2} + \frac{\partial^2 C}{\partial y^2} + \frac{\partial^2 C}{\partial z^2}\right)$$
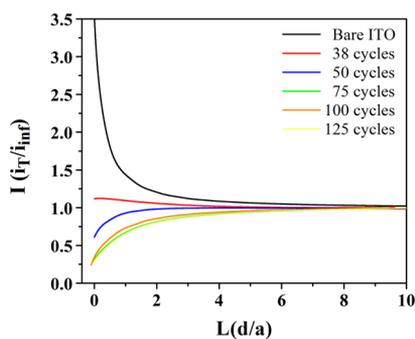
Figure 6. SECM approach curves on substrates with different surface coverage. The solution is 1 mM FcMeOH in 0.1 M KNO$_3$. 10 μm Pt tip electrode. Scan rate = 500 nm s^{-1}. $E_{tip} = 0.5$ V, $E_{subs} = 0.0$ V.

where the diffusion coefficient is $D = 7.8 \times 10^{-6}$ cm^2 s^{-1}.[42] For an inlaid macroelectrode, like the one depicted in Figure 2A, the current response recorded under mass transfer control follows Cottrell behavior (eq 1, red line in Figure 2D). However, representing the ALD partial surface coverage of TiO$_2$ on the ITO substrates as a regular array of pores (Figure 2B), the current response with time is a function of the three main parameters illustrated in Figure 2C: the radius of the pores produced, r_p; the center-to-center distance separation between such pores, d_{c-c}; and the net length of the microarray, l_{arr}. For example, a microarray like the one depicted in Figure 2B with 49 pores, $r_p = 37.5$ μm, $d_{c-c} = 5r_p$, and $l_{arr} = 600$ μm, produces a simulated response similar to the chronoamperogram obtained after 25 ALD pulses of TiO$_2$ on ITO, as shown in Figure 2D (black line). At times $t \leq r_p^2/D$ or ~10 s for the example here, semi-infinite linear diffusion controls mass transfer at each individual UME (pinhole) present on the substrate. At longer times, e.g., $t > 10$ s, the currents at each UME transitions to steady-state and the magnitude of $\log_{10} i(t)$ tends toward leveling off. However, at $t > d_{c-c}^2/D$ or ~100 s, the diffusion layers of all pinholes overlap to give a second transition to linear diffusion, this one characteristic of a single electrode with area l_{arr}^2. The model was validated by performing chronoamperometric measurements on substrates having surface architectures similar to the ones considered in the numerical simulations (see Experimental Section and Supporting Information Figure S8). The comparison between experimental currents and those obtained from the FEM model are shown in Figure 3.

Additional simulations were carried out with other parameters, varying r_p, d_{c-c}, and the number of pinholes to understand the behavior of the ALD transients in Figure 1. These are summarized in Table 2. To represent these ALD chronoamperometric results, it is convenient to plot the current at a given time as a function of the number of ALD cycles. A typical plot for
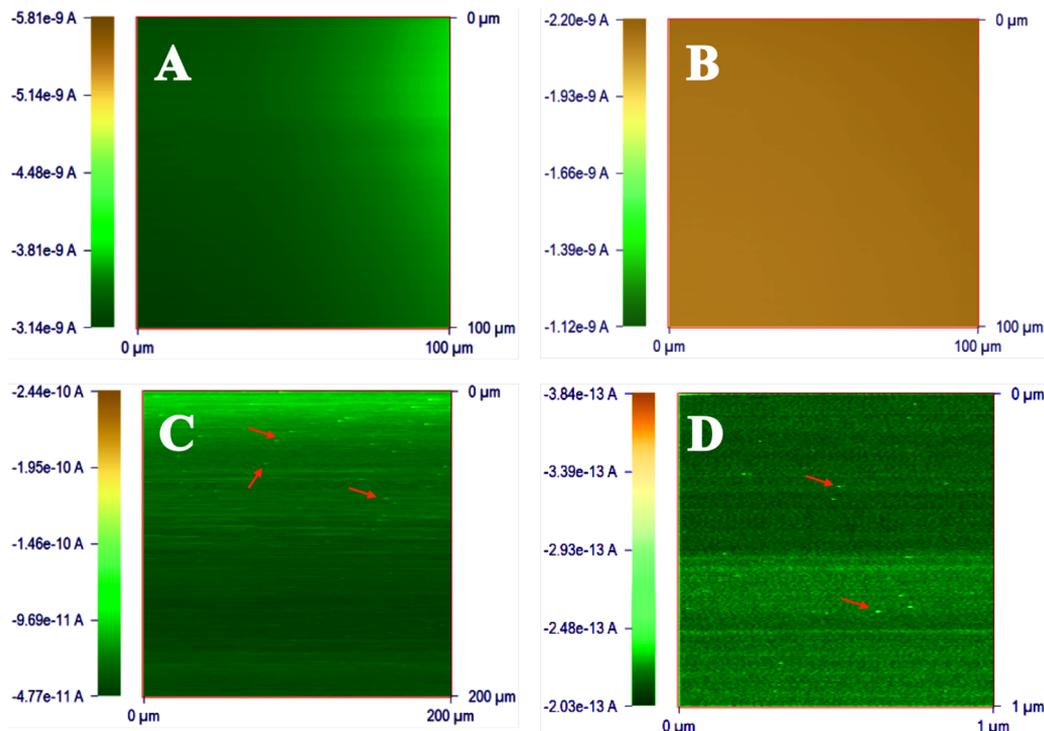
Figure 7. SECM images taken above substrates with (A) 25 ALD cycles; (B) 50 ALD cycles; (C) 75 ALD cycles; and (D) 100 ALD cycles of TiO$_2$ on ITO.

$t = 100$ s, i.e., $i(t = 100$ s$)$ vs number of ALD deposition cycles is presented in Figure 4 (extracted from Figure 1 as indicated by the vertical dashed line). Figure 4 shows how the anodic current recorded at $t = 100$ s remained constant up to about 25 deposition cycles, with a magnitude close to the current recorded on bare ITO under similar conditions. This behavior is indicative of exposed ITO zones that are sufficiently close that the diffusion layers over them overlap. Above 25 cycles with continuing TiO_2 coverage the current decreased as expected by the pinhole model. However, close to complete coverage of the ITO surface was only achieved after about 100 deposition cycles, with recorded currents still in the nA scale. This represents a few pinholes in the 4 to 5 nm thick TiO_2 film that remained and behaved as isolated UMEs. Mathematical fitting of the data shown in Figure 4 was achieved with a sigmoidal function at a correlation of $R^2 = 0.994$.

Voltammetric Analysis. As an alternative to chronoamperometry, cyclic voltammetry experiments were carried out using each of the TiO_2-covered samples prepared as a working electrode by fixing them to a SECM cell in substrate configuration (diameter of the exposed surface was 5 mm). Oxidation of ferrocenemethanol was used to obtain cyclic voltammograms (CVs) to study TiO_2 coverage as a function of number of ALD cycles applied. The CVs are shown in Figure 5. The principle of the behavior is analogous to that of the chronoamperometry, with oxidation of FcMeOH at the bare ITO electrode at $v = 20$ mV s^{-1} showing macroelectrode mass transfer behavior that gradually shifts to UME CV as the number of ALD cycles increases. The magnitude of ΔE_p on the bare ITO increased from 88 mV (uncorrected for iR-drop) with increasing scan rate. ALD deposition of TiO_2 at 25 cycles produced a larger peak-potential separation, $\Delta E_p = 147$ mV at $v = 20$ mV s^{-1}, even though there was a 50% decrease in the anodic current. This suggests that the reaction on ITO is somewhat sluggish with resulting in higher overpotentials at the higher current densities of the partially covered film. Similar behavior was observed at 38 cycles. With >50 cycles, the scan rate dependence transitioned from linear to spherical diffusion. This confirms that the substrates can now be described by UME pinholes that do not interact with one another. Spherical diffusion was especially evident at the larger number of deposition cycles, particularly above 100. Furthermore, as the number of deposition cycles increased, the anodic current was reduced progressively to a minimum reached at 125 cycles, with a value 2 orders of magnitude smaller than that corresponding to the bare ITO substrate. The decrease in the magnitude of the anodic current and the presence of spherical diffusion indicate that the pores present in the deposits were progressively filled up with an increasing number of deposition cycles. If one assumes that the 125th cycle response is due to a single circular pore, its radius would be ≈ 700 μm.

Evaluation by SECM. The ALD samples were also examined by SECM with FcMeOH as the mediator. Approach curves were recorded for a substrate potential of 0.0 V, where reduction of FcMeOH$^+$ is diffusion controlled, as shown in Figure 6; in these a 10 μm diameter Pt UME tip approached the TiO_2-coated ITO sample immersed in 1 mM FcMeOH + 0.1 M KNO_3 solution. The feedback response is interpreted as follows: when the tip potential is sufficiently positive that the oxidation of FcMeOH is diffusion-controlled (e.g., at 0.5 V), the feedback is positive when the tip is over a region (>~25 μm in size) of ITO that is free of any blocking TiO_2 film. However, when the tip is over a TiO_2 region, negative feedback is
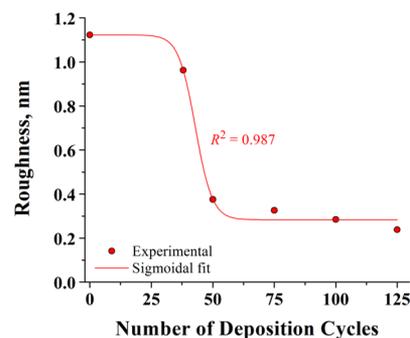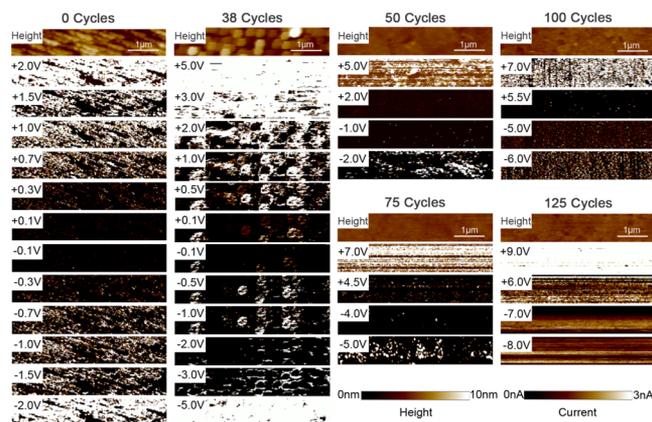
Figure 8. Top. Atomic force micrographs (height) and conductive atomic force microscope images of electrical current magnitude (labeled by tip−sample bias voltage) for ITO substrate ("0 cycles") and 38, 50, 75, 100, and 125 cycles of TiO_2 deposition on ITO. For each sample, the topographic and current images are acquired from the same area of the sample surface. As the number of TiO_2 deposition cycles is increased, the overall current conduction through the TiO_2 layer decreases and the spatial distribution of the observed current undergoes a transition from being highly localized (38 and 50 cycles) to being more uniformly distributed across the sample surface (100 and 125 cycles). The height scale for all topographic images is 0−10 nm and the current magnitude scale for all current images is 0−3 nA. Bottom. Plot of roughness vs number of ALD deposition cycles for TiO_2 on ITO. Surface roughness was evaluated as the root-mean-square (RMS) value of the distribution of heights in the cAFM topographical images.

observed. A third case must be considered when the tip is over a region that contains both conductive ITO and insulating TiO_2 regions within roughly the diameter of the tip; the feedback curve will then be between the limiting pure positive and pure negative feedback and will depend on the relative amounts of both. This technique has been used previously, e.g., to examine gold electrodes covered by self-assembled alkyl thiol monolayers.[43,44] In the case of the bare ITO substrate, pure negative feedback was observed. Approach curves recorded on deposits produced with 25 ALD cycles presented essentially the same behavior as that of the bare ITO sample (these results are not shown), indicating with this that there were many small holes that diffusively interacted on the surface covered with TiO_2. However, when the ITO substrate was treated with 38 deposition cycles, a 3 times decrease in positive feedback was observed. This result indicated that more extensive coverage of TiO_2 was achieved at that point, and that this coverage started to be homogeneously distributed over the ITO surface. With further increase in the number of deposition cycles to 50, 75,
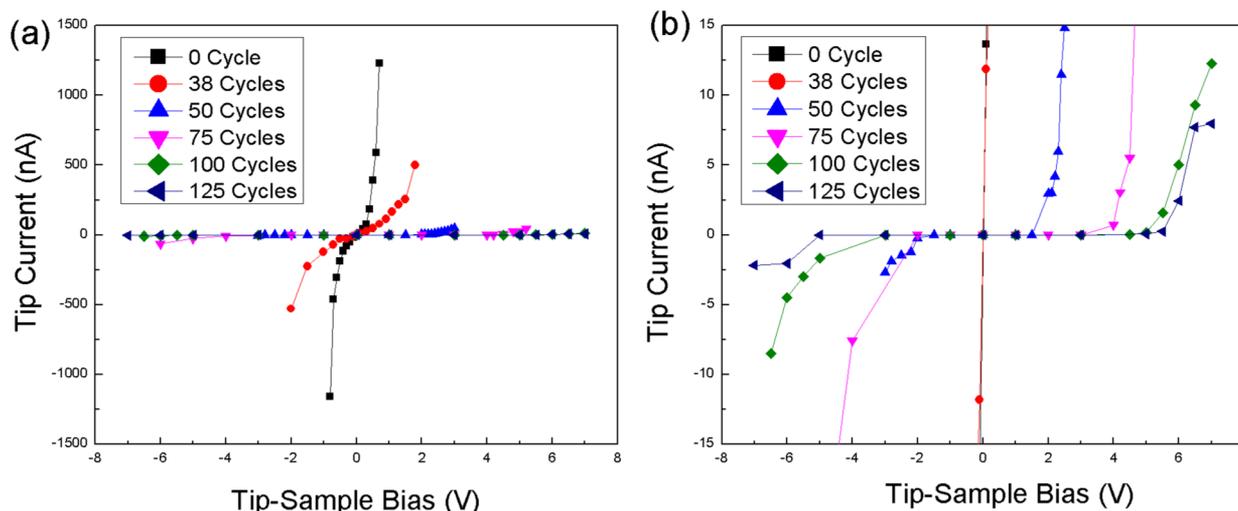
Figure 9. Current−voltage spectra extracted from 10 μm × 10 μm conductive AFM images of local current flow. Spectra are shown for the ITO substrate (0 cycles) and samples consisting of 38, 50, 75, 100, and 125 cycles of TiO$_2$ deposition on ITO. Current levels shown are obtained by averaging the measured current in each image and are plotted on current scales of (a) large current range and (b) small current range.

100, and 125, negative feedback behavior was progressively observed until full negative feedback was attained at 125 cycles. In general, these observations indicate that TiO$_2$ deposition at small numbers of ALD cycles (<30 cycles) produces films with sufficient porosity to provide complete positive feedback to the tip. On the other hand, increasing the number of deposition cycles favors pore filling and limits the rate of electron transfer.

SECM Imaging of Film Defects. SECM images of four different substrates with 25, 50, 75, and 100 ALD cycles were taken to confirm the existence of defects in the TiO$_2$ films. The first three images were recorded at a distance $d \approx 2$ μm above the substrates, with a 10 μm diameter Pt tip (RG = 2.0 ± 0.1). The last image was taken at $d \approx 37$ nm with an 86 nm diameter Pt tip (see Experimental Section and Supporting Information Figures S9 and S10). Again, 1 mM FcMeOH in 0.1 M NaNO$_3$ was used as the electrochemical probe. Substrates corresponding to the two lowest numbers of deposition cycles presented a very high current background, and the images obtained were featureless, as presented in Figure 7A,B. The lack of features indicates that the area beneath the tip had both small open and insulating spots, so the recorded current represents the average of both, as previously seen with SAM films by SECM. The gradation seen probably represents a substrate leveling effect with a small difference in d at the left and right edges. Note the average current of A is much larger than that of B. However, when the films corresponding to 75 cycles were imaged, high current density spots were detected (see examples at the red arrows in Figure 7C). Such spots may not correspond to individual defects present in the film but rather to groups of imperfections with merged diffusion layers (i.e., the resolution of the tip was only able to resolve aggregations of defects at $d \approx 2$ μm). The existence of such bright spots was also an indication that at a lower number of deposition cycles the deposits were highly porous and that the individual diffusion layers of the defects present in the films were merged. At 75 deposition cycles different aggregations of pores were well separated, allowing detection by the 10 μm Pt tip. At a number of deposition cycles equal to or larger than 100, the pores became too small to be detected by the 10 μm Pt tip, so a nanoelectrode was needed. In the last image, the low current background obtained with such an electrode allowed the detection of bright spots of only a

few nanometers in diameter. This resolution of such small individual pores in a 1 μm by 1 μm scan is the highest yet attained by SECM.

Conductive AFM. cAFM measurements were employed to probe electrical current conduction through the TiO$_2$ layer at the nanoscale as a function of TiO$_2$ thickness. Figure 8 shows atomic force microscope topographic and current images for 1 μm × 5 μm areas of the ITO substrate and of 38, 50, 75, 100, and 125 cycles of TiO$_2$ deposited on ITO. For each sample, the topographic and current images were obtained from the same area of the sample surface. The ITO surface is, as expected, found to be highly conductive with relatively uniform spatial distribution of electrical current flow across the sample surface. For 38 cycles of TiO$_2$ deposition, we observe that the onset of current flow at low voltages is highly localized spatially, with the current flow eventually occurring through the entire sample surface at higher voltages. We attribute the localized nature of current flow at low voltages to variations in thickness in the initially deposited TiO$_2$ layer, with elevated electrical conduction occurring in regions with minimal or no TiO$_2$ coverage. Indeed, peak local current flow measured for the 38th cycle TiO$_2$ sample is comparable to or greater than that for the ITO sample, suggesting that defects with no TiO$_2$ coverage exist in that sample. Localization of current flow decreases with increasing TiO$_2$ deposition, with the samples for which 100 or 125 cycles of TiO$_2$ were deposited showing fairly uniform spatial distributions for current flow. Figure 9 shows the average current flow per point extracted from conductive atomic force microscope images of the ITO substrate and of samples with 38, 50, 75, 100, and 125 cycles of TiO$_2$ deposited on ITO. As expected, the average current level decreases dramatically with increasing TiO$_2$ deposition. The averaged currents presented in Figure 9 are higher than the currents seen in Figure 8 because of the existence of "current hot-spots" on the samples. Statistical analysis was carried out to demonstrate this (Supporting Information Figure S11).

■ **CONCLUSION**

The present work presents a complete electrochemical characterization of the ALD deposition process of TiO$_2$ on ITO as a function of the number of ALD cycles applied.

The characterization was carried out by chronoamperometry, voltammetry, SECM, and cAFM. Our results demonstrate that the deposits of TiO$_2$ produced by ALD are porous in nature, and fairly complete blocking films require >~90 cycles. Furthermore, the porosity of such deposits decreases with increasing number of deposition cycles performed. Chronoamperometric evaluation of the films demonstrated that electron transfer happens at surface defects, and the use of numerical simulations indicate behavior similar to that seen on arrays of microelectrodes. Good agreement existed between simulated data and experimental results with representative arrays.

■ ASSOCIATED CONTENT

Ⓢ Supporting Information

Additional SEM, XPS, CV, and experimental data. This material is available free of charge via the Internet at http://pubs.acs.org.

■ AUTHOR INFORMATION

Corresponding Author
*E-mail: ajbard@mail.utexas.edu (A.J.B.).

Present Address
†Bhabha Atomic Research Centre, Trombay, Mumbai-400085, India (A.K.S.).

Author Contributions
‡Authors contributed equally (A.K.S. and N.A.-C.).

Notes
The authors declare no competing financial interest.

■ ACKNOWLEDGMENTS

■ REFERENCES

(1) *Scanning Electrochemical Microscopy*, 2nd ed.; Bard, A. J., Mirkin, M. V., Eds.; CRC Press: Boca Raton, FL, 2012.

(2) Suntola, T.; Hyvarinen, J. *Annu. Rev. Mater. Sci.* **1985**, *15*, 177−195.

(3) Kiani, A.; Alpuche-Aviles, M. A.; Eggers, P. K.; Jones, M.; Gooding, J. J.; Paddon-Row, M. N.; Bard, A. J. *Langmuir* **2008**, *24*, 2841−2849.

(4) Suntola, T.; Antson, J. U.S. Patent 4058430, 1977.

(5) George, S. M. *Chem. Rev.* **2010**, *110*, 111−131.

(6) International Technology Roadmap for Semiconductors. Atomic Layer Deposition. http://www.itrs.net/ (accessed Dec. 17, 2012).

(7) Sneh, O.; Clark-Phelps, R. B.; Londergan, A. R.; Winkler, J.; Seidel, T. E. *Thin Solid Films* **2002**, *402*, 248−261.

(8) Kim, S. K.; Lee, S. W.; Han, J. H.; Lee, B.; Han, S.; Hwang, C. S. *Adv. Funct. Mater.* **2010**, *20*, 2989−3003.

(9) Leskelä, M.; Ritala, M. *J. Phys. (Paris)* **1999**, *9*, 837−852.

(10) Kwon, J.; Dai, M.; Halls, M. D.; Langereis, E.; Chabal, Y. J.; Gordon, R. G. *J. Phys. Chem. C* **2009**, *113*, 654−660.

(11) Abdel-Fattah, T. M.; Gu, D.; Baumgart, H.; Bajpai, R.; Zaghloul, M. *ECS Trans.* **2009**, *25*, 93−99.

(12) Hsu, I. J.; McCandless, B. E.; Weiland, C.; Willis, B. G. *J. Vac. Sci. Technol. A* **2009**, *27*, 660−667.

(13) McDaniel, M. D.; Posadas, A.; Wang, T.; Demkov, A. A.; Ekerdt, J. G. *Thin Solid Films* **2012**, *520*, 6525−6530.

(14) Triyoso, D.; Liu, R.; Roan, D.; Ramon, M.; Edwards, N. V.; Gregory, R.; Werho, D.; Kulik, J.; Tam, G.; Irwin, E.; Wang, X. D.; La, L. B.; Hobbs, C.; Garcia, R.; Baker, J.; White, B. E.; Tobin, P. *J. Electrochem. Soc.* **2004**, *151*, 220−227.

(15) Schmitt, S. W.; Gamez, G.; Sivakov, V.; Schubert, M.; Christiansen, S. H.; Michler, J. *J. Anal. At. Spectrom.* **2011**, *26*, 822−827.

(16) Chen, Y. W.; Prange, J. D.; Dühnen, S.; Park, Y.; Gunji, M.; Chidsey, C. E. D.; McIntyre, P. C. *Nat. Mater.* **2011**, *7*, 539−544.

(17) Aarik, J.; Aidla, A.; Sammelselg, V.; Siimon, H.; Uustare, T. *J. Cryst. Growth* **1996**, *169*, 496−502.

(18) Puurunen, R. L. *J. Appl. Phys.* **2005**, *97*, 121301.

(19) George, S. M. *Chem. Rev.* **2010**, *110*, 111−131.

(20) Knez, M.; Nielsch, K.; Niinistö, L. *Adv. Mater.* **2007**, *19*, 3425−3438.

(21) Goodman, C. H. L.; Pessa, M. V. *J. Appl. Phys.* **1986**, *60*, R65.

(22) Suntola, T. *Mater. Sci. Rep.* **1989**, *4*, 261.

(23) Niinistö, L.; Ritala, M.; Leskela, M. *Mater. Sci. Eng.* **1996**, *B41*, 23.

(24) Malygin, A. A.; Malkov, A. A.; Dubrovenskii, S. D. *Stud. Surf. Sci. Catal.* **1996**, *99*, 213.

(25) Ritala, M.; Leskelä, M. *Handbook of Thin Film Materials*; Nalwa, H. S., Ed.; Academic: San Diego, CA, 2002; Vol. 1, pp 103−159.

(26) Haukka, S.; Lakomaa, E. L.; Suntola, T. *Stud. Surf. Sci. Catal.* **1999**, *120A*, 715.

(27) Leskela, M.; Ritala, M. *Angew. Chem., Int. Ed.* **2003**, *42*, 5548−5554.

(28) Hausmann, D. M.; Kim, E.; Becker, J.; Gordon, R. G. *Chem. Mater.* **2002**, *14*, 4350−4358.

(29) Norton, E. T., Jr.; Amato-Wierda, C. *Chem. Mater.* **2001**, *13*, 4655−4660.

(30) Xie, Q.; Jiang, Y. L.; Detavernier, C.; Deduytsche, D.; Meirhaeghe, R. L. V.; Ru, G. P.; Li, B. Z.; Qua, X. P. *J. Appl. Phys.* **2007**, *102*, 083521.

(31) Xia, Y.; Whitesides, G. M. *Angew. Chem., Int. Ed.* **1998**, *37*, 550−575.

(32) Chow, K.; Mavre, F.; Crooks, J. A.; Chang, B.; Crooks, R. M. *J. Am. Chem. Soc.* **2009**, *131*, 8364−8365.

(33) *Electrochemical Methods: Fundamentals and Applications*; Bard, A. J., Faulkner, L. R.; Wiley: New York, NY, 2000; pp 624−628.

(34) Weaver, M. J. Redox Reactions at Metal-Solution Interfaces. In *Comprehensive Chemical Kinetics*; Compton, R. G., Ed.; Elsevier: Amsterdam, 1987; Vol. 27, Chap. 1.

(35) Davies, J. T.; Ward-Jones, S.; Banks, C. E.; Del Campo, J.; Mas, R.; Muñoz, F. X.; Compton, R. G. *J. Electroanal. Chem.* **2005**, *585*, 51−62.

(36) Davies, T. J.; Compton, R. G. *J. Electroanal. Chem.* **2005**, *585*, 63−82.

(37) Zoski, C. G.; Yang, N. *Anal. Chem.* **2007**, *79*, 1474−1484.

(38) Guo, J.; Lindner, E. *Anal. Chem.* **2009**, *81*, 130−138.

(39) Manshykau, D.; Huang, X.; Rees, N. V.; Del Campo, F. J.; Munoz, F. X.; Compton, R. G. *Analyst* **2009**, *134*, 343−348.

(40) Zoski, C. G.; Wijesinghe, M. *Isr. J. Chem.* **2010**, *50*, 347−359.

(41) Beriet, C.; Ferrigno, R.; Girault, H. H. *J. Electroanal. Chem.* **2000**, *486*, 56−64.

(42) Miao, W.; Ding, Z.; Bard, A. J. *J. Phys. Chem. B* **2002**, *106*, 1392−1398.

(43) Forouzan, F.; Bard, A. J.; Mirkin, M. V. *Isr. J. Chem.* **1997**, *37*, 155−163.

(44) Wittstock, G.; Hesse, R.; Schuhmann, W. *Electroanalysis* **1997**, *9*, 746−750.